Deterministic Josephson vortex ratchet with a load

M. Knufinke,[1] K. Ilin,[2] M. Siegel,[2] D. Koelle,[1] R. Kleiner,[1] and E. Goldobin[1]

[1]*Physikalisches Institut–Experimentalphysik II and Center for Collective Quantum Phenomena in LISA*$^+$*, Universität Tübingen, Auf der Morgenstelle 14, D-72076 Tübingen, Germany*

[2]*Universität Karlsruhe, Institut für Mikro- und Nanoelektronische Systeme, Hertzstraße 16, D-76187 Karlsruhe, Germany*

(Received 29 September 2011; published 13 January 2012)

We investigate experimentally a deterministic underdamped Josephson vortex ratchet—a fluxon particle moving along a Josephson junction in an asymmetric periodic potential. By applying a sinusoidal driving current, one can compel the vortex to move in a certain direction, producing an average dc voltage across the junction. Being in such a rectification regime, we also load the ratchet, i.e., apply an additional dc bias current I_{dc} (counterforce) which tilts the potential so that the fluxon climbs uphill due to the ratchet effect. The value of the bias current at which the fluxon stops climbing up defines the strength of the ratchet effect and is determined experimentally. This allows us to estimate the loading capability of the ratchet, the output power, and the efficiency. For the quasistatic regime we present a simple model which delivers straightforward analytic expressions for the above-mentioned figures of merit.

DOI: 10.1103/PhysRevE.85.011122 PACS number(s): 05.45.−a, 05.40.−a, 85.25.Cp, 74.50.+r

I. INTRODUCTION

The discovery of Brownian motion suggested the idea of extracting useful work out of random motion. As Feynman *et al.* demonstrated [1], drawing energy from equilibrium thermal fluctuations (white noise) is forbidden by the second law of thermodynamics. The extraction of work out of *nonequilibrium* or time-correlated noise (colored noise) is possible using ratchet systems [2–5]. Such systems, which either incorporate an asymmetric periodic potential or are subjected to a drive with temporal asymmetry [6,7], have been in the focus of attention during the last two decades in various implementations. In particular, superconducting systems based on the motion of Josephson vortices [8–17], Abrikosov vortices [18–20], or the Josephson phase in superconducting quantum interference devices (SQUIDs) [21–26] have been suggested and tested experimentally.

Josephson ratchets have some advantages over other ratchet systems: (I) directed motion results in an average dc voltage which makes ratchet operation easily accessible in experiment; (II) Josephson junctions are very fast devices, i.e., they can be operated in a broad frequency range from dc up to 100 GHz, which allows them to capture a lot of spectral energy; (III) both underdamped and overdamped systems can be investigated by proper junction design and the variation of the bath temperature. We note that, although (I) also applies to Abrikosov vortex ratchets, (II) and (III) do not. Abrikosov vortex ratchets offer the advantage of studying directed motion in two-dimensional potentials. However, typically they cannot compete with Josephson devices in terms of either performance or a simple model that describes them.

The deterministic underdamped Josephson vortex ratchet (JVR) in which a Josephson vortex (fluxon) moves along a long Josephson junction (LJJ) was implemented earlier [16]. A strongly asymmetric tunable potential was created using a current injector [10,16]. The periodicity of the potential is provided by the annular geometry of the LJJ [27–30]. The fluxon was injected into the annular LJJ also in a controllable way using a pair of tiny current injectors [31,32]. The directional motion of a fluxon was detected by measuring the (averaged) dc voltage across the junction, which is, due to the Josephson relation, proportional to the average velocity of a fluxon, and reached values as high as $0.9\bar{c}_0$, where $\bar{c}_0$ is the Swihart velocity (maximum possible velocity of a fluxon). However, in these experiments the JVR was idle, i.e., was not delivering any rectified power to a load.

In this paper we investigate several figures of merit of such a JVR relevant for applications: the rectification window, maximum dc counterforce against which the ratchet can still work, output power, and efficiency in both quasistatic and nonadiabatic regimes. The paper is organized as follows: In Sec. II we describe the equations for the dynamics of the Josephson phase in a LJJ with a ratchet potential created by an injector current. The sample design and characterization are presented in Sec. III. Experimental and analytical results for quasistatic driving frequencies are presented in Sec. IV. Section V covers experimental and numerical results for the nonadiabatic drive. Section VI concludes this work.

II. THEORY

Our system consists of an annular long Josephson junction (ALJJ) equipped with injectors to create an asymmetric potential and to insert a fluxon; see Fig. 1. The dynamics of the Josephson phase in the system can be described by the following perturbed sine-Gordon equation [10]:

$$\phi_{xx} - \phi_{tt} - \sin\phi = \alpha\phi_t - \gamma - \gamma_{\rm inj}(x) - \xi(t), \qquad (1)$$

where $\phi(x,t)$ is the Josephson phase and subscripts x and t denote derivatives with respect to space and time, respectively. The curvilinear coordinate x along the LJJ is normalized to the Josephson penetration depth λ_J and the time t is normalized to the inverse of the plasma frequency ω_p^{-1}. The quantity α is the dimensionless damping parameter. $\gamma = j/j_c$, $\gamma_{\rm inj}(x) = j_{\rm inj}(x)/j_c$, and $\xi(t) = j(t)/j_c$ are the dc bias current density, injector current density, and ac driving current density, respectively, all normalized to the critical current density j_c of the LJJ. $\gamma_{\rm inj}(x)$ has zero spatial average and is used to create an asymmetric potential; γ is used to apply an additional dc bias

 ©2012 American Physical Society

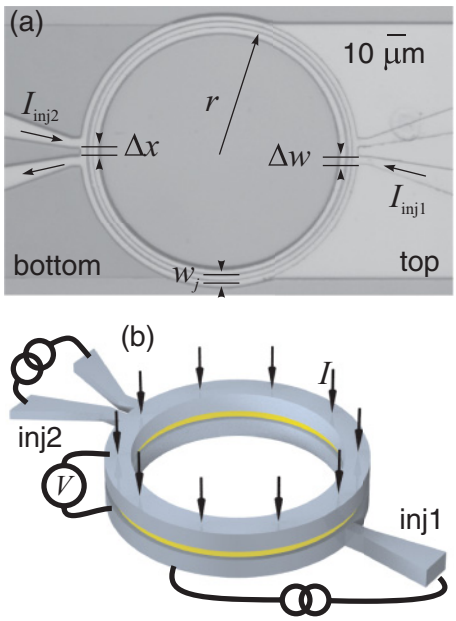

FIG. 1. (Color online) (a) Optical image of the ALJJ used in our experiments. Only one injector of the right pair is used. (b) Sketch of the ALJJ with a single injector 1 and a double injector 2. Bias leads for top and bottom electrodes are not shown for clarity.

current while the device is operated in the rectification regime (see below). $\xi(t)$ is a spatially homogeneous deterministic (or stochastic) drive with zero time average. The ultimate aim of ratchet operation is to rectify $\xi(t)$ to produce a nonzero voltage $\overline{V} \propto \overline{\phi_t} \neq 0$, which is independent of x.

In the absence of the right-hand side, the solitonic solution of Eq. (1) is a Josephson vortex (sine-Gordon kink) $\phi(x) = 4\arctan(\exp\{[x - x_0(t)]/\sqrt{1-u^2}\})$ situated at x_0 and moving with velocity $u = dx_0(t)/dt$ [33]. The right-hand side of Eq. (1) is usually considered as a perturbation [34]. It does not drastically change the vortex shape, but defines its dynamics, e.g., its equilibrium velocity [34]. Such an approximation essentially treats the vortex as a rigid object, and its dynamics can be reduced to the dynamics of a relativistic underdamped pointlike particle [11] (cf. the nonrelativistic case [35]). In these terms, the ratchet should rectify $\xi(t)$ to produce a nonzero average velocity $\overline{u} \neq 0$.

We implement the asymmetric potential using a single injector (further called inj1); see Fig. 1. A suitable current profile $\gamma_{inj}(x)$ is equivalent to a nonuniform magnetic field $h(x)$ along the LJJ, such that $\gamma_{inj}(x) = -h_x(x)$. The normalized potential $U(x_0)$ experienced by a fluxon particle is given by $U(x_0) \approx -2\pi(w_J/\lambda_J)h(x_0)$, where w_J is the junction width [10].

Such a profile can be realized by applying a current γ_{inj} through a single injector of width Δw situated at $x = x_{inj1}$ and extracting the current over the same electrode along the rest of the LJJ, i.e.,

$$\gamma_{inj}(x) = \begin{cases} \gamma_1 & \text{for } |x - x_{inj1}| < \Delta w/(2\lambda_J), \\ \gamma_2 & \text{otherwise}, \end{cases} \tag{2}$$

such that $\gamma_1 \Delta w + \gamma_2(L - \Delta w) = 0$ with the ALJJ circumference $L = 2\pi r$, where r is the mean radius of the ALJJ. In this case, $U(x_0)$ looks like an asymmetric sawtooth potential with the steep slope proportional to γ_1 and the gentle slope proportional to γ_2, i.e., the asymmetry depends on the width Δw compared to the junction length L; see Fig. 1. The amplitude of the potential can be varied by changing $I_{inj1} = \gamma_1 \Delta w w_J$, which, in principle, also allows the operation as a flashing ratchet. Here, we focus on the rocking ratchet only, i.e., the potential proportional to γ_{inj1} is (almost) constant and $\xi(t) \neq 0$. To apply the current I_{inj1} we use one of the two injectors visible in Fig. 1. The injector is attached to the bottom electrode. The current I_{inj1} is injected via inj1 into the bottom electrode of the ALJJ and is used to create the asymmetric potential as described above.

The periodicity of the potential is provided by using an annular LJJ and $\langle \gamma_{inj}(x) \rangle_x = 0$. Note that the latter condition is automatically satisfied because I_{inj1} is applied to the same electrode so that $\gamma_1 j_c \Delta w w_J = \gamma_2 j_c (L - \Delta w) w_J = I_{inj1}$.

In addition, our JVR has a pair of current injectors (further called inj2) separated by a distance Δx and attached to the top superconducting electrode; see Fig. 1. They are used to insert a fluxon (Josephson vortex) in the ALJJ [31,32].

III. SAMPLES

We investigated several Nb-Al-AlO_x-Nb junctions with different parameters. Here, we report the results obtained for two samples with parameters summarized in Table I. For all samples, $\lambda_J \gg w_J = 5\ \mu$m and $\lambda_J \gg \Delta w = \Delta x$ (see Table I), i.e., we can treat our ALJJs as one dimensional and inj2 as an ideal discontinuity [32]. The maximum revolution frequency for a fluxon inside an ALJJ equals $\nu_0 = \overline{c}_0/L$ with the Swihart velocity $\overline{c}_0$. The corresponding voltage (voltage of the first fluxon step) is given as

$$V_1 = \Phi_0 \nu_0 = \Phi_0 \omega_p / l \tag{3}$$

with the normalized length $l = L/\lambda_J$.

All measurements have been performed at the temperature $T = 4.2$ K. All junctions showed good I-V characteristics (IVCs) and symmetric $I_c(H)$ dependences (not shown). Their $I_c(I_{inj2})$ dependences look Fraunhofer-like, in agreement with the theory [32]. The first minimum of this dependence corresponds to the phase being twisted by $\pm 2\pi$ in a tiny region between the injector pair inj2 and to a free (anti)fluxon being inserted into the ALJJ region outside inj2. Thus, we insert a fluxon into the junction by choosing the corresponding value of I_{inj2}.

To calibrate inj1, we measure $I_c(I_{inj1})$ (see Fig. 2). By measuring $I_c(I_{inj1})$ without a fluxon inside the junction ($I_{inj2} = 0$) and comparing it to $I_c(I_{inj1})$ measured with a fluxon inside

TABLE I. Parameters of the used junctions. r is the junction radius, j_c is the critical current density at 4.2 K, λ_J is the Josephson penetration depth, and l is the normalized junction length. Δx and Δw describe the injector seperation and width (see text).

Sample	r (μm)	j_c (A/cm^2)	λ_J (μm)	l	$\Delta x = \Delta w$ (μm)
C3	70	87	47	9.4	5
E3	30	138	29	6.5	2

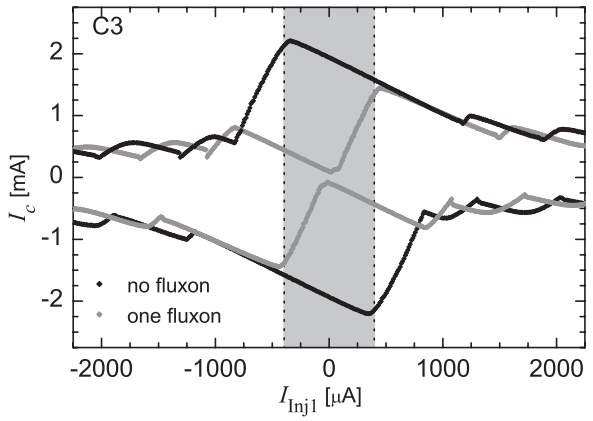

FIG. 2. $I_c(I_{\mathrm{inj1}})$ dependence for sample C3. The range of I_{inj1} relevant for ratchet operation, i.e., the region where the picture of a fluxon particle moving in a potential is valid, is shaded.

the junction ($I_{\mathrm{inj2}} \propto \Delta\phi = \pm 2\pi$), the asymmetry of the ratchet is determined and the range of I_{inj1} (range of the amplitude of the ratchet potential) relevant to the ratchet operation is found [10,16]; see Fig. 2. Inside this working range, the depinning current I_c scales almost linearly with I_{inj1}, but it is asymmetric for positive and negative directions of the bias current I (driving force). Note, that as in Ref. [16], a residual pinning of the fluxon due to the finite inj2 sizes Δx and Δw is still visible in Fig. 2 [32].

When the IVC is measured with a fluxon inside the junction and $I_{\mathrm{inj1}} \neq 0$, i.e., an applied ratchet potential, a fluxon step appears on the IVC (not shown) corresponding to the rotation of a fluxon around the ALJJ with $u \approx \bar{c}_0$. The depinning currents I_c and return currents I_r of the fluxon step depend on the polarity of the applied bias as well as on I_{inj1}.

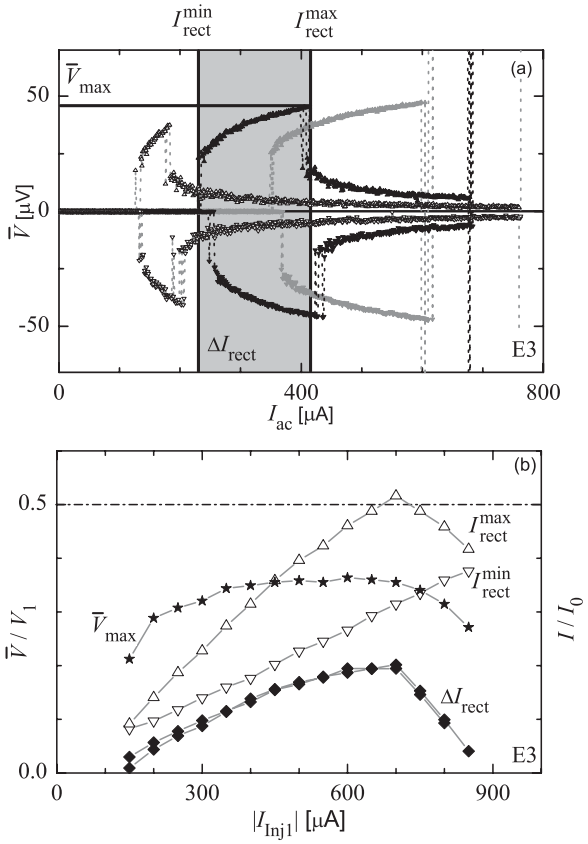

FIG. 3. (a) Typical rectification curves $\overline{V}(I_{\mathrm{ac}})$ for $I_{\mathrm{inj1}} = \pm 200$, ± 400, and ± 600 μA (open, black, and gray symbols, respectively). (b) Figures of merit for different potential amplitudes normalized to I_0 and V_0, respectively. ΔI_{rect} is shown for both positive and negative potential amplitude.

IV. QUASISTATIC DRIVE

For our experiments in the quasistatic regime, we apply a periodic bias current $I(t) = \xi(t) j_c L w_J = I_{\mathrm{ac}} \sin(2\pi\nu t)$ with the frequency $\nu = 100$ Hz $\ll \nu_0$ and measure the rectification curve $\overline{V}(I_{\mathrm{ac}})$ by averaging the voltage over 10 ms (1000 data points sampled at 100 kHz)—one period of the ac drive. For the junction E3 the dependence $\overline{V}(I_{\mathrm{ac}}) = V_1 \overline{u}(I_{\mathrm{ac}})$ is shown in Fig. 3(a) for different values of I_{inj1}, i.e., for different amplitudes of the potential. Note that the absolute maximum $\overline{V}$, which can be obtained with a rectangular-shaped driving force, is given by $0.5V_1$, because the fluxon is driven only half a period in one direction. For a sinelike driving force, as in our case, the maximum voltage is somewhat smaller [10].

All $\overline{V}(I_{\mathrm{ac}})$ curves show similar features. For small I_{ac} the driving force acting on a fluxon is not sufficient to push the fluxon out of the potential well in either direction so that $\overline{u} \propto \overline{V} = 0$. At $I_{\mathrm{ac}} > I^{\mathrm{min}}_{\mathrm{rect}}$ the bias is able to push the fluxon in one direction but not in the other, which results in $\overline{u} \propto \overline{V} \neq 0$. At $I_{\mathrm{ac}} > I^{\mathrm{max}}_{\mathrm{rect}}$, the junction switches into the resistive state, generating a high positive or negative dc voltage. The latter regime is not discussed here as it has nothing to do with the JVR operation. Rarely, we also observed the typical ratchet behavior—a decrease of $\overline{V}$ at $I_{\mathrm{ac}} > I^{\mathrm{max}}_{\mathrm{rect}}$ when the driving force is able to overcome the potential barrier in both directions and rectification thus drops significantly. We rarely observe this regime since the asymmetry is so large that a negative fluxon step does not appear in most cases.

For not very large potential heights proportional to I_{inj1}, i.e., when the perturbation theory is applicable, the values $I^{\mathrm{min}}_{\mathrm{rect}}$ and $I^{\mathrm{max}}_{\mathrm{rect}}$ grow approximately linearly with I_{inj1}; see Fig. 3(b). Therefore, the size of the rectification window $\Delta I_{\mathrm{rect}} = I^{\mathrm{max}}_{\mathrm{rect}} - I^{\mathrm{min}}_{\mathrm{rect}}$ also grows approximately linearly with I_{inj1}. Further, V_{max} grows with I_{inj1}, but it reaches its maximum value already for medium values of I_{inj1}; see Fig. 3(b). At high potential amplitudes the rectification window is becoming smaller, probably because the ratchet potential cannot be considered anymore as a perturbation.

The dependence shown in Fig. 3(b) is qualitatively the same for all measured samples and for both signs of the potential, as long as the junction length l is large enough. For $l \lesssim 4$ the asymmetry of the potential is strongly reduced because the potential is a convolution of the magnetic field profile created by inj1 and the fluxon shape [10]. The main result of Fig. 3(b) is that, in order to obtain large V_{max} and large ΔI_{rect}, one should operate the ratchet at large amplitudes of the potential, i.e., at large values of I_{inj1}.

In the quasistatic regime, all information about the ratchet operation can be derived from its IVC. Therefore, we can derive all figures of merit that we are interested in by using the

model steplike IVC shown in Fig. 4(a), which is very similar to a real one. In this IVC, which we express as

$$V_{\mathrm{mod}}(I) = V_1 \times \begin{cases} -1, & I < I_{c-}, \\ 0, & I_{c-} < I < I_{c+}, \\ +1, & I_{c+} < I, \end{cases} \tag{4}$$

the fluxon depinning currents $I_{c+} > 0$ and $I_{c-} < 0$ have different values reflecting the asymmetry of the potential. The fluxon step is roughly approximated by a vertical step with infinite height. The applied current $I(t) = I_{\mathrm{dc}} + I_{\mathrm{ac}} \sin(\omega t)$ consists of a dc current and an ac current with frequency ω.

To obtain a rectification curve $\overline{V}(I_{\mathrm{ac}})$, we integrate the instant voltage over one period $T = 2\pi/\omega$ of ac drive, i.e.,

$$\overline{V}(I_{\mathrm{ac}}) = \frac{1}{T} \int_0^T V_{\mathrm{mod}}[I(t)]\, dt. \tag{5}$$

Within our simple model, this can be integrated explicitly, resulting in

$$\overline{V} = \begin{cases} 0, & I_{\mathrm{ac}} < I_{c+} - I_{\mathrm{dc}}, \\ V_+, & I_{c+} - I_{\mathrm{dc}} < I_{\mathrm{ac}} < I_{\mathrm{dc}} - I_{c-}, \\ V_+ + V_-, & I_{\mathrm{dc}} - I_{c-} < I_{\mathrm{ac}}, \end{cases} \tag{6}$$

where

$$V_+ = \frac{+1}{2\pi}\left[\pi + 2 \arcsin\left(\frac{I_{\mathrm{dc}} - I_{c+}}{I_{\mathrm{ac}}}\right)\right], \tag{7a}$$

$$V_- = \frac{-1}{2\pi}\left[\pi - 2 \arcsin\left(\frac{I_{\mathrm{dc}} - I_{c-}}{I_{\mathrm{ac}}}\right)\right] \tag{7b}$$

describe the part of $\overline{V}$ rectified during the positive and the negative semiperiod of ac drive, respectively.

The $\overline{V}(I_{\mathrm{ac}})$ calculated in this way is shown in Fig. 4(b). First, for $I_{\mathrm{dc}} = 0$ our simple model gives $I_{\mathrm{rect}}^{\mathrm{min}} = I_{c+}$, $I_{\mathrm{rect}}^{\mathrm{max}} = -I_{c-}$, and $\Delta I_{\mathrm{rect}} = -I_{c-} - I_{c+}$. For the chosen values of $|I_{c-}| > |I_{c+}|$ the rectified voltage $\overline{V} \geqslant 0$.

Second, we apply I_{dc} to try to stop the ratchet operation at a given value of I_{ac}. The sign of I_{dc} should be opposite to the sign of $\overline{V}$, i.e., $I_{\mathrm{dc}} < 0$ in our case. Rectification curves $\overline{V}(I_{\mathrm{ac}})$ calculated using Eq. (6) at different values of $I_{\mathrm{dc}} < 0$ are also shown in Fig. 4(b). One can see that the rectification window shrinks, i.e., close to the edges of the original window the ratchet is not strong enough to work against I_{dc}. With applied I_{dc}

$$I_{\mathrm{rect}}^{\mathrm{min}} = I_{c+} - I_{\mathrm{dc}}, \tag{8}$$

$$I_{\mathrm{rect}}^{\mathrm{max}} = I_{\mathrm{dc}} - I_{c-}, \tag{9}$$

$$\Delta I_{\mathrm{rect}} = 2I_{\mathrm{dc}} - I_{c-} - I_{c+}, \tag{10}$$

which can also be seen from Eq. (6).

One can also take a different point of view and study how strong the ratchet is at each particular I_{ac}, i.e., one varies I_{dc} at fixed I_{ac}. The value of I_{dc} at which the ratchet stops moving or starts moving backward ($\overline{V} = 0$ or changes sign) is called the stopping force (or stopping current) I_{stop}. The dependence $I_{\mathrm{stop}}(I_{\mathrm{ac}})$ is shown in Fig. 4(f). One can see that naturally $I_{\mathrm{stop}} = 0$ up to the driving amplitude $I_{\mathrm{ac}} = I_{c+}$, because the ratchet has not started working yet, so no force is needed to stop it. Then I_{stop} grows linearly to a value of $I_{\mathrm{stop}}^{\mathrm{max}} = \Delta I_{\mathrm{rect}}/2 = (-I_{c-} - I_{c+})/2$, which is reached at

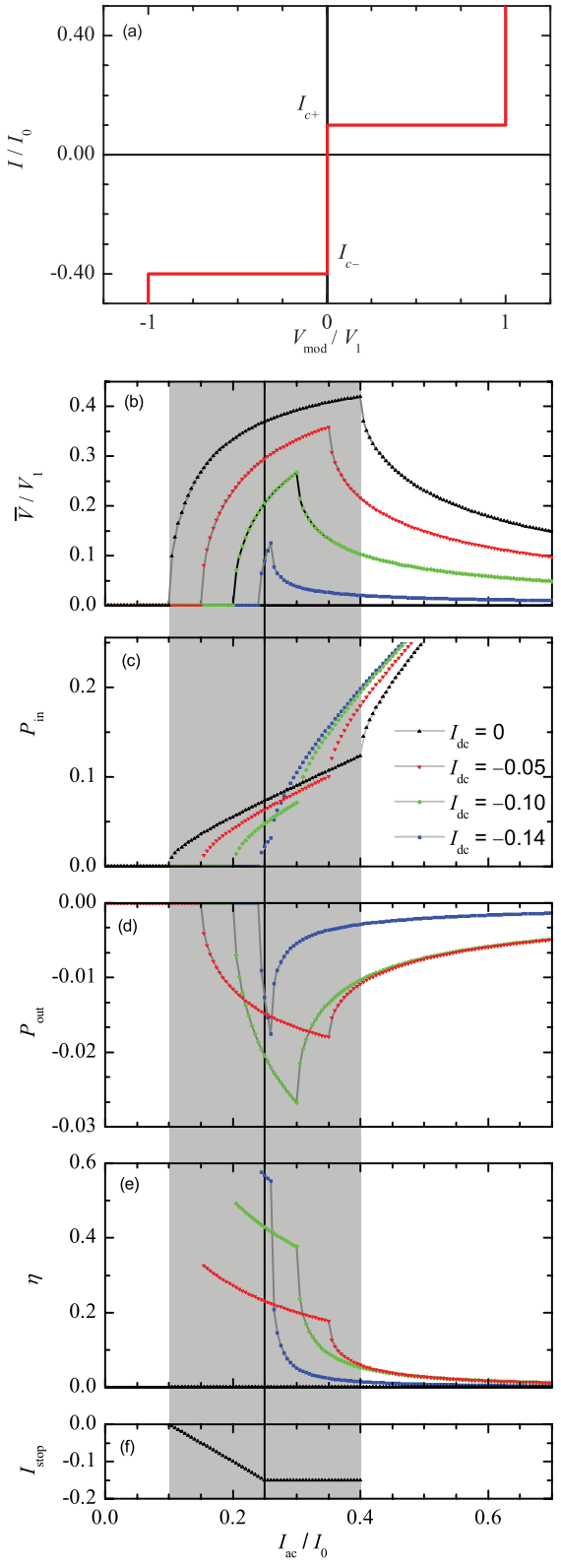

FIG. 4. (Color online) (a) Model step-function-like IVC (4) with $I_{c+} = 0.1I_0$ and $I_{c-} = -0.4I_0$; $I_0 = j_c w_J L$ is the intrinsic critical current. (b) $\overline{V}(I_{\mathrm{ac}})$ curves calculated using Eq. (6). (c) $P_{\mathrm{in}}(I_{\mathrm{ac}})$ [Eq. (15)]. (d) $P_{\mathrm{out}}(I_{\mathrm{ac}})$ [Eq. (13)]. (e) Power efficiency $\eta = -P_{\mathrm{out}}/P_{\mathrm{in}}$ for different values of $I_{\mathrm{dc}} = 0, -0.05, -0.10, -0.14$. (f) $I_{\mathrm{stop}}(I_{\mathrm{ac}})$; see Eqs. (11) and (12) with saturation value $I_{\mathrm{stop}} = -0.15$ [Eq. (12)].

$I_{ac} = (-I_{c-} + I_{c+})/2$, i.e., at the middle of the rectification window. In this regime, the ratchet rectifies because during some fraction of the positive semiperiod $I(\tau)$ exceeds I_{c+} and never exceeds I_{c-}; see Fig. 4(a). An additional I_{dc} "shifts" the origin of ac oscillations down along the I axis. Thus, for $I_{dc} < |I_{ac}| - I_{c+}$, the ac sweep does not exceed the depinning current I_{c+} and rectification vanishes. Therefore

$$I_{stop} = |I_{ac}| - I_{c+} \quad \text{for} \quad |I_{ac}| > I_{c+}, \tag{11}$$

which corresponds to the linear part in Fig. 4(f). The behavior described by Eq. (11) does not hold for arbitrarily large I_{ac}. When $|I_{ac}| > (I_{c+} - I_{c-})/2$, at some amplitude of I_{dc} the ac sweep also exceeds the negative depinning current I_{c-}, which results in a drastic decrease of rectification and also I_{rect}^{max} given by Eq. (9); see Fig. 4(b). At $I_{dc} = (I_{c-} + I_{c+})/2$, the ac sweep experiences symmetric depinning currents and rectification vanishes. Thus

$$I_{stop} = (I_{c-} + I_{c+})/2 \quad \text{for} \quad |I_{ac}| > (I_{c+} - I_{c-})/2, \tag{12}$$

corresponding to a saturation of I_{stop} in Fig. 4(f) and a completely closed rectification window on the $\overline{V}(I_{ac}, I_{stop})$ plot. For $I_{dc} < (I_{c-} + I_{c+})/2$, the rectified voltage $\overline{V}$ changes sign.

Let us now discuss the power balance in our ratchet. Since $I_{dc} = \text{const}$, the average dc output power

$$P_{out} = \frac{1}{T}\int_0^T V(t) I_{dc}\, dt = \overline{V} I_{dc} \leqslant 0, \tag{13}$$

where $\overline{V}(I_{ac}, I_{dc})$ is given by Eq. (6). P_{out} is negative because the ratchet delivers the power to the dc source (load) instead of consuming it. Simultaneously, the input power is given by

$$P_{in} = \frac{1}{T}\int_0^T V(t) I_{ac} \sin(\omega t)\, dt \geqslant 0. \tag{14}$$

Within our simple model, this can be integrated explicitly, resulting in

$$P_{in} = \begin{cases} 0, & I_{ac} < I_{c+} - I_{dc}, \\ P_{in}^{+}, & I_{c+} - I_{dc} < I_{ac} < I_{dc} - I_{c-}, \\ P_{in}^{+} + P_{in}^{-}, & I_{dc} - I_{c-} < I_{ac}, \end{cases} \tag{15}$$

where

$$P_{in}^{+} = \frac{1}{\pi I_{ac}}\sqrt{I_{ac}^2 - (I_{dc} - I_{c+})^2}, \tag{16a}$$

$$P_{in}^{-} = \frac{1}{\pi I_{ac}}\sqrt{I_{ac}^2 - (I_{dc} - I_{c-})^2} \tag{16b}$$

describe the part of P_{in} consumed during the positive and the negative semiperiod of ac drive, respectively.

Both $P_{in}(I_{ac})$ and $P_{out}(I_{ac})$ at different values of I_{dc} are shown in Figs. 4(c) and 4(d). One can see that $P_{in}(I_{ac})$ has two characteristic branches corresponding to the dissipation during the positive semiperiod and during both the positive and negative semiperiods. In contrast, $P_{out}(I_{ac})$ is nonmonotonic and has an extremum given by

$$\overline{V}\left[I_{rect}^{max}(I_{dc})\right] I_{dc} = I_{dc}\left[\frac{1}{2} + \frac{1}{\pi}\arcsin\left(\frac{I_{dc} - I_{c+}}{I_{dc} - I_{c-}}\right)\right] \tag{17}$$

at $I_{ac} = I_{rect}^{max}(I_{dc})$ [Eq. (9)], which depends on I_{dc} nonmonotonically. One can see that $P_{out} = 0$ not only at $I_{dc} = 0$, but also at $I_{dc} = I_{stop}$ where $\overline{V} = 0$; cf. Eq. (13). Therefore, the maximum power is reached for some intermediate values of $I_{stop} < I_{dc} < 0$. The exact value can be derived by looking for the extremum of expression (17) with respect to I_{dc}. It is reached for I_{dc}^{opt}, which is a solution of the following transcendental equation:

$$\left(\frac{I_{c+} - I_{c-}}{I_{dc}^{opt} - I_{c-}}\right)\frac{I_{dc}^{opt}}{\pi} + \left[\frac{1}{2} + \frac{1}{\pi}\arcsin\left(\frac{I_{dc}^{opt} - I_{c+}}{I_{dc}^{opt} - I_{c-}}\right)\right] \times \sqrt{1 - \left(\frac{I_{dc}^{opt} - I_{c+}}{I_{dc}^{opt} - I_{c-}}\right)^2} = 0. \tag{18}$$

For our parameters, $I_{dc}^{opt} \approx -0.104 I_0$ and $P_{max}(I_{dc}^{opt}) = -0.028 V_1 I_0$.

Another important figure of merit is the efficiency, defined as $\eta = -P_{out}/P_{in}$. The plots $\eta(I_{ac})$ are shown in Fig. 4(e). Obviously, the efficiency has a maximum just at the beginning of the rectification window and falls with increasing $|I_{dc}|$. To derive the approximate behavior of $\eta(I_{ac})$ at the beginning of the rectification window analytically, we Taylor-expand P_{out} and P_{in} near $I_{ac} = I_{rect}^{min}(I_{dc})$ [Eq. (8)]. As a result, we get

$$\eta(I_{ac}, I_{dc}) \approx \frac{I_{dc}}{I_{dc} - I_{c+}} - \frac{1}{6}\frac{I_{dc}}{(I_{dc} - I_{c+})^2}\left(I_{ac} - I_{rect}^{min}\right). \tag{19}$$

The first term represents the exact expression for the efficiency at the left edge of the rectification window for given I_{dc}. To find the maximum efficiency, we vary I_{dc} from 0 down to $I_{stop}^{max} = (I_{c+} + I_{c-})/2$. At $I_{dc} \to I_{stop}^{max}$, the efficiency approaches it ultimate maximum value

$$\eta_{max} = \frac{I_{c-} + I_{c+}}{I_{c-} - I_{c+}}, \tag{20}$$

although the rectification window ΔI_{rect} vanishes; see Figs. 4(b)–4(e). For our values of I_{c-} and I_{c+} (see the caption of Fig. 4) $\eta_{max} = 0.6$.

V. NONADIABATIC DRIVE

We use a microwave generator with an emitting antenna close to the ALJJ to drive the ratchet at frequencies as high as $\nu \gtrsim 1$ GHz. With this geometry, the bias leads of the ALJJ act as a pickup antenna. Note that the microwaves are also picked up by the injector electrodes but due to the geometry of the setup this causes only a negligible "flashing" part in our ratchet behavior [16]. We average the dc voltage $\overline{V}$ over 2000 data points at a sampling rate of 100 kHz ($\sim 10^8$ periods) and measure it vs the applied power $P \propto I_{ac}$ of the generator.

Rather than growing smoothly as in Fig. 3(a), the rectified voltage $\overline{V}$ is now quantized as

$$\overline{V}_n = -\,\text{sgn}\,(I_{inj1}) n \Phi_0 \nu \tag{21}$$

(Shapiro-like steps) [10]. Each step corresponds to an integer number n of turns of a fluxon around the ALJJ per one period of the ac drive. The prefactor $-\text{sgn}\,(I_{inj1})$ is chosen so that $n > 0$ corresponds to the motion of a fluxon in the "easy" direction of the potential, while $n < 0$ corresponds to the difficult direction (particle's current-reversal, which, in our particular setup, corresponds to voltage reversal); cf. Fig. 2. If the time τ_0 required for one revolution of a fluxon around the

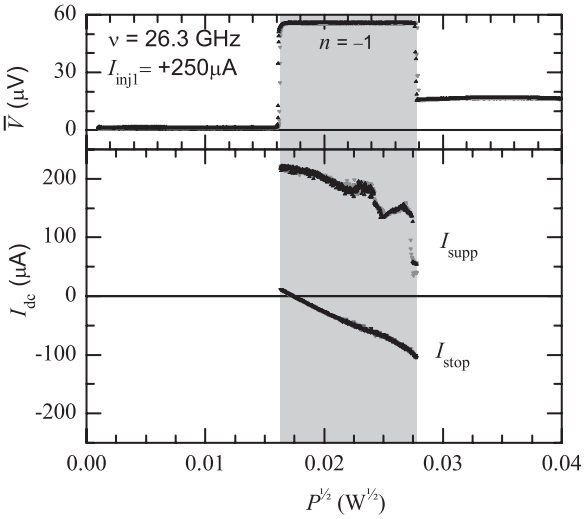

FIG. 5. Rectification curve with positive potential sign. Stopping force $I_{stop}(P)$ and support force $I_{supp}(P)$. Black triangles: P is swept up; gray triangles: P is swept down.

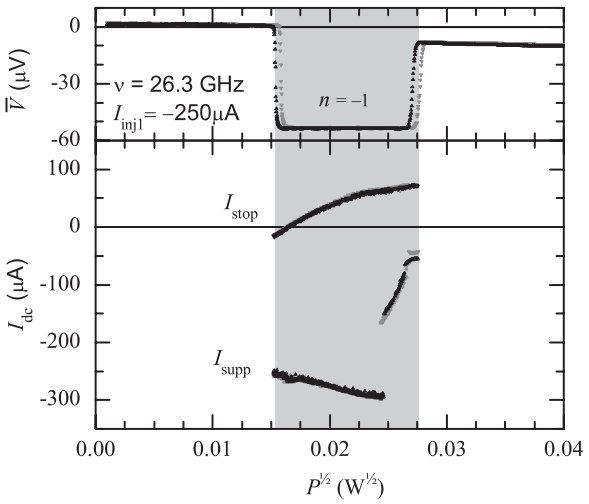

FIG. 6. Rectification curve with negative potential sign. Stopping force $I_{stop}(P)$ and support force $I_{supp}(P)$. Black triangles correspond to sweep up, gray triangles to sweep down.

ALJJ (in the best case $\tau_0 = \bar{c}_0/L$) becomes comparable with the period of the driving force, i.e., if the voltage $\overline{V} = \Phi_0\nu$ is approaching V_1, the fluxon has time for only one revolution, so $n = 1$ and only one step can be observed on the $\overline{V}(P)$ curves. In the nonadiabatic regime, current reversal can also be observed, i.e., $n = -1$ resulting in a "negative" voltage [36–40].

Being in the rectification regime, we apply an additional bias current I_{dc} which tries either to stop the ratchet operation (i.e., with sign opposite to $\overline{V}$) or to "help" it (i.e., with the same sign as $\overline{V}$). In the nonadiabatic regime it makes sense to associate I_{stop} and I_{supp} with a particular mode of operation (step n) rather than with the ratchet as a whole. Therefore, a particular mode of operation is ending when the voltage $\overline{V}(I_{dc} \neq 0) \neq \overline{V}(I_{dc} = 0)$. The value of I_{dc} at which this condition is met is called the *stopping force* $I_{stop}(P)$ or *support force* $I_{supp}(P)$ respectively.

Figure 5 shows a typical rectification curve measured using the sample C3 at $I_{dc} = 0$. The voltage step corresponds to $n = -1$. In addition, we show the $I_{stop}(P)$ and $I_{supp}(P)$ dependences for this area. Figure 6 shows the curves for the same parameter setting, but with the potential amplitude reversed in comparison to Fig. 5.

The rectification curves $\overline{V}(I_{ac})$ show the expected discrete values of rectified voltage. An inverted potential causes an inverted voltage step. Different sweeping directions of P result in almost identical curves, which suggests that we are not observing a simple synchronization of the fluxon movement with the drive (for which we can lock to the $n = \pm 1$ step randomly) but rather a true rectification with well-defined direction independent of the history. We check this for every voltage step to ensure that we are observing a real ratchet effect and also measure I_{stop} and I_{supp} for different sweeping directions to avoid regimes of synchronization.

In both plots, $I_{stop} = 0$ at the lower edge of the rectification window—a feature that we observe in almost all measurements. From this point, the stopping force I_{stop} grows smoothly throughout the rectification window. It vanishes when we leave the rectification regime of $n = -1$.

The support force I_{supp} also looks similar in both plots (but with opposite sign). It has a minimum value at the upper edge of the rectification window. At lower driving amplitudes I_{supp} stays ≈const and drops very fast (or even jumps abruptly) down to its minimum at the upper edge of the rectification window.

The maximum value of I_{stop} in all our measurements was $|I_{stop}^{max}| = 215\ \mu A = 0.112 I_0$ (reached at the edge of the rectification window) and $|I_{supp}^{max}| = 298\ \mu A = 0.155 I_0$ (both in sample C3, not shown). Note that $|I_{supp}^{max}| > |I_{stop}^{max}|$ in all measurements.

In sample E3, we observed both direct rectification ($n = +1$) and reversal ($n = -1$) in one rectification curve at a driving frequency $\nu = 16.9$ GHz; see Fig. 7(a). The voltage jumps directly from one step to the other, showing a small hysteresis (indicated by the arrows) when P is swept back and forth. We measured $I_{stop}(P)$ and $I_{supp}(P)$ for both voltage steps. Also note the data point at $\sqrt{P} \approx 0.0048\sqrt{W}$. The step with $n = -1$ is metastable in the interval $\sqrt{P} = (0.0054{-}0.0057)\sqrt{W}$, so one can see the system jump there sometimes.

Figure 7(b) shows $I_{stop}(P)$ and $I_{supp}(P)$ for $n = +1$. The shape of $I_{stop}(P)$ is similar to the previous plots. In the middle of the rectification window, the curve gets more noisy and, at the upper edge, I_{stop} shows a small hysteresis for different sweep directions of P. $I_{supp}(P)$ is almost constant throughout the major part of the plot and jumps close to the upper edge of the rectification window.

Figure 7(c) shows I_{stop} and I_{supp} for the step $n = -1$. $I_{supp}(P)$ has a well-known shape—the curve remains at high values within the whole rectification window. The $I_{stop}(P)$ curve vanishes at *both* ends of the rectification window. In fact, one can see that it consists of two branches that join at a value of driving amplitude where the voltage step $n = -1$ is ending, i.e., the left branch of $I_{stop}(P)$ shows rectification with $n = -1$, although the $\overline{V}(P)$ curve has switched already to $n = +1$ dynamics in this region. The reason is that we are tracking the $n = -1$ mode, which is not visible for $I_{dc} = 0$, but appears for $I_{dc} \neq 0$. The fact that we can track it shows

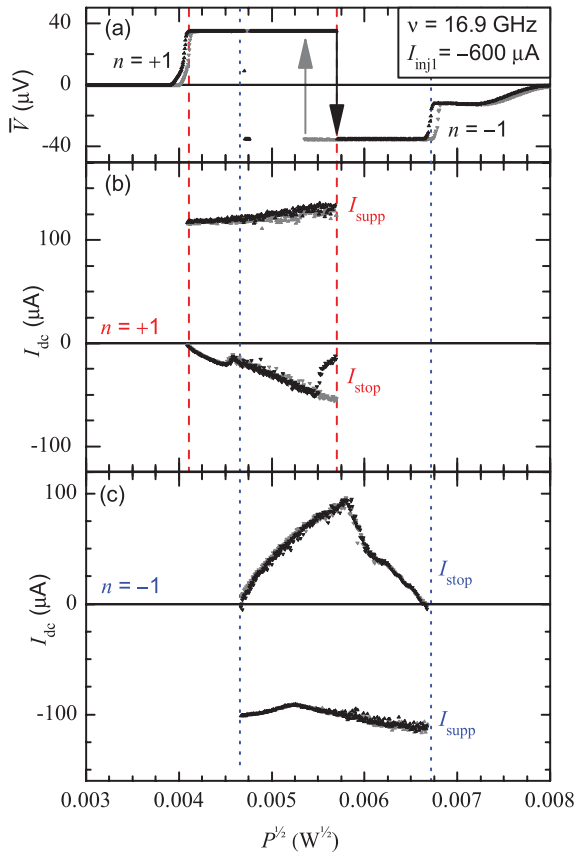

FIG. 7. (Color online) Rectification curve for $\nu = 16.9$ GHz (a). Stopping force $I_{stop}(P)$ and support force $I_{supp}(P)$ for voltage step corresponding to $n = +1$ (b) and $n = -1$ (c).

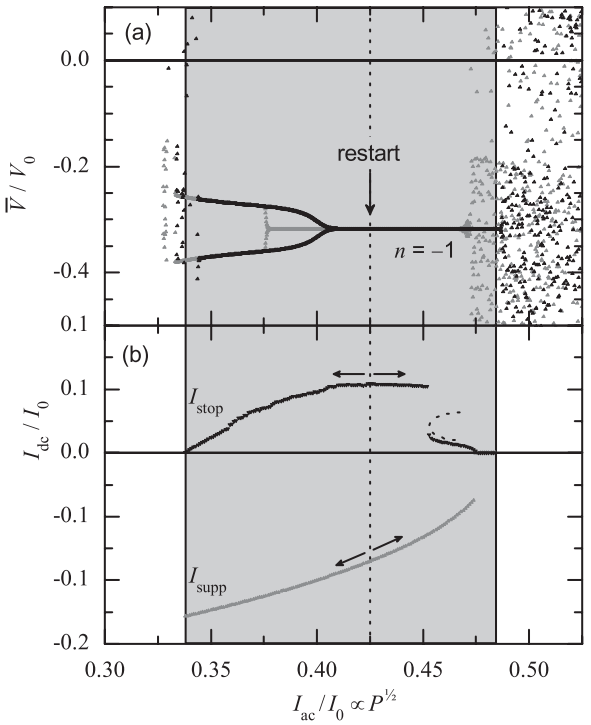

FIG. 8. (a) Numerically simulated $\overline{V}(I_{ac})$ for ALJJ of $l = 8.0$ and driving frequency $\omega/\omega_{pl} = 0.25$. Black data points correspond to sweeping I_{ac} upward, and the gray points to a downward sweep. The value of I_{ac} where the simulation is restarted (see text) is indicated by the dotted line. (b) $I_{stop}(I_{ac})$ and $I_{supp}(I_{ac})$ for the voltage step corresponding to $n = -1$. Black (gray) symbols correspond to positive (negative) sweeping direction of I_{ac}. I_{stop} is reduced by a region of instability (marked by the dashed line).

that the presence of the $n = -1$ mode depends on the history of the system and the value of I_{dc} in a nontrivial way.

The reason for this might be the measurement itself: For the measurement of $\overline{V}(P)$, the current $I_{dc} = \text{const} \approx 0$ (a small current offset is always possible), while for the measurement of $I_{stop}(P)$ or $I_{supp}(P)$ the current I_{dc} is ramped up for each amplitude of the drive P and then set to $I_{dc} \approx 0$ again for the next value of P. This subtle difference can influence the fluxon dynamics inside the junction and therefore the $n = -1$ dynamics can apply for longer than was seen in the rectification curve. In this sense, the measurement of the stopping force or support force can be used for further investigation of possible modes of operation while measuring the loading capability of the ratchet.

For the nonadiabatic regime, numerical simulations show a behavior similar to the experimental results (for the quasistatic regime, these simulations are very time consuming and can be avoided by using an analytical approach similar to the one discussed in Sec. IV). These simulations were performed using an explicit numerical scheme for Eq. (1) with damping coefficient $\alpha = 0.1$ (weakly underdamped limit). The numerical technique and simulation software are discussed in detail in [41].

In Fig. 8 we show simulated $\overline{V}(I_{ac})$ as well as $I_{stop}(I_{ac})$ and $I_{supp}(I_{ac})$ dependences. In our simulation of $\overline{V}(I_{ac})$ dependences shown in Fig. 8, the sweep of I_{ac} was performed from $0.3I_0$ to $0.6I_0$ and back. The value of $\overline{V}$ was calculated by averaging V only over *one period* of ac drive. Therefore, if we are in the chaotic regime, we will observe a finite value of the voltage in our simulation, while in the experiment these will be averaged to some finite value which is often equal to zero. The chaotic voltage distribution in Fig. 8 at $I_{ac} > 0.48$ shows such a chaotic regime. For this simulation, the (discrete) step in I_{ac} was chosen very tiny so that the system still has time to come into equilibrium, although one sees the transient processes in $\overline{V}(I_{ac})$. A large discrete change of the system parameters (e.g., the driving power or I_{dc}) may give a different result than a small one, i.e., the resulting value of I_{stop} or I_{supp} can be much smaller than for smooth parameter changes. This happens because the dynamics is close to chaotic and thus even a small kick (steplike change of parameters) may drive the system into a different state. Our simulations use a small step size of $10^{-5}I_0$.

Then, for the simulation of $I_{stop}(I_{ac})$ and $I_{supp}(I_{ac})$ we started by recalling the state of the system at $I_{ac}/I_0 = 0.425$ (where rectification takes place) and then sweeping I_{ac} into each direction and, for given I_{ac}, looking for I_{stop} or I_{supp}. For the interpretation of the plots, the curves at $I_{ac} < 0.425$ have to be interpreted by looking at the $\overline{V}(I_{ac})$ curve swept in the negative direction, while $I_{stop}(I_{ac})$ and $I_{supp}(I_{ac})$ at $I_{ac} > 0.425$ have to be followed looking at the positive sweep of $\overline{V}(I_{ac})$.

The $\overline{V}(I_{ac})$ curve reproduces the $n = -1$ step observed in the experiment; cf. Figs. 5 and 6. At $0.34 < I_{ac} < 0.41$

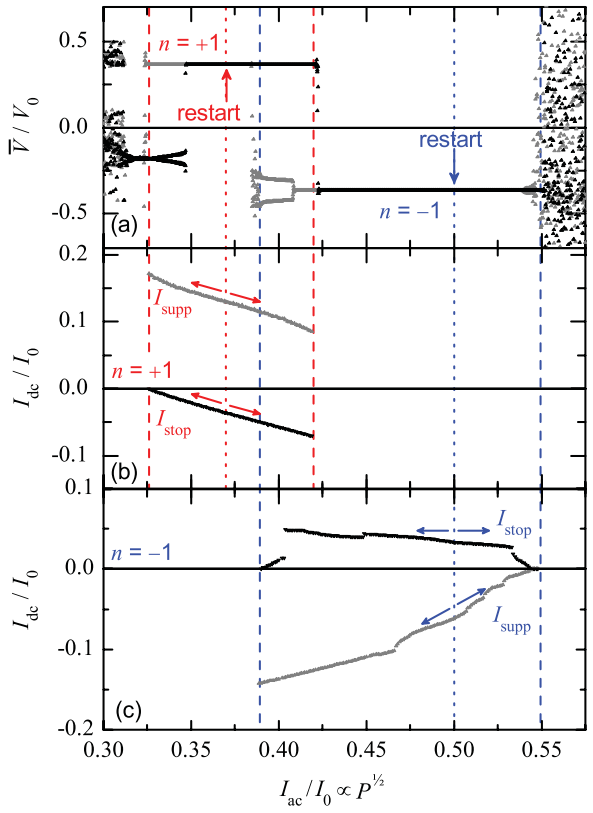

FIG. 9. (Color online) (a) Numerically simulated $\overline{V}(I_{ac})$ for ALJJ of $l = 10.0$ and driving frequency $\omega/\omega_{pl} = 0.23$. Black data points correspond to sweeping I_{ac} upward, and the gray points to a downward sweep. (b) $I_{stop}(I_{ac})$ and $I_{supp}(I_{ac})$ for the voltage step corresponding to $n = +1$. Black (gray) symbols correspond to positive (negative) sweeping direction of I_{ac}.

one can see period-2 dynamics in the $\overline{V}(I_{ac})$ curve. Again, this can be observed only in simulations as these values are averaged to their mean in our experiment. One can see that the $I_{stop}(I_{ac})$ curve is similarly shaped as in our measurement (see Fig. 6), showing an increasing value at larger driving power. At high driving amplitudes, one can see a jump in the $I_{stop}(I_{ac})$ curve to lower values of I_{stop}, which we did not see in our particular measurement. This jump is related to the presence of an island in the I_{dc}-I_{ac} plane (marked by the dashed line) where the dynamics is not $n = -1$ anymore. The $I_{supp}(I_{ac})$ curve shows large values over the whole rectification window. We believe that in our experiment we also meet the island where the solution for $n = -1$ is not stable.

We have also been able to reproduce a situation in which both $n = +1$ and $n = -1$ dynamics are present on one rectification curve as in our measurements on sample E3. The corresponding numerical simulation results for a LJJ of the normalized length $l = 10.0$ are presented in Fig. 9(a).

In this simulation, the sweep of I_{ac} was performed also from $0.3I_0$ to $0.6I_0$ and back with the same step in I_{ac} as in Fig. 8(a). For the interpretation of the plots, for $I_{ac} < 0.50I_0$ one has to refer to the $\overline{V}(I_{ac})$ curve swept in the negative direction; for $I_{ac} > 0.50$ the positive sweep of $\overline{V}(I_{ac})$ has to be followed.

In Fig. 9(a) the transition between the voltage steps $n = +1$ and $n = -1$ shows a small hysteresis. Moreover, for the negative sweeping direction of I_{ac}, a bifurcation to period-2 dynamics is visible. In our experiment with much longer integration time, this is averaged to the same step voltage and is not distinguishable from period-1 dynamics. The same applies to the region (outside the $n = \pm 1$ voltage steps) where the system shows chaotic dynamics—due to the averaging in our experiments, one observes just an average voltage of the chaotic fluxon motion.

Figure 9(b) shows the $I_{stop}(P)$ and $I_{supp}(P)$ dependences for the $n = +1$ step. They confirm the behavior observed in our measurements. Namely, the stopping force $I_{stop}(I_{ac})$ grows almost linearly from the lower edge of the rectification window to larger values and then jumps down to zero. The support force $I_{supp}(I_{ac})$ also shows the well-known behavior and drops smoothly to smaller values on approaching the upper edge of the rectification window.

Figure 9(c) shows the $I_{stop}(P)$ and $I_{supp}(P)$ dependences for $n = -1$. They look very similar to those measured using the sample E3; cf. Fig. 7(c). The stopping force $I_{stop}(I_{ac})$ also grows from the lower edge of the rectification window and at some point jumps to a branch growing from the upper edge—in our simulation, the curves also show a jump. This jump is located at a driving amplitude I_{ac} where the rectification curve $\overline{V}(I_{ac})$ has a bifurcation and is right inside the hysteretic area. The support force $I_{supp}(I_{ac})$ again drops to lower values with increasing driving amplitude I_{ac} and goes down to zero at the upper edge of the rectification window. One can see that the curve consists of several pieces that may be related to switching into different dynamical regimes. This is in contrast to the experimental results where $I_{supp}(I_{ac})$ falls abruptly down to zero.

The maximum values $I_{stop}^{max} = 0.049I_0$ and $I_{supp}^{max} = 0.167I_0$ in Figs. 9(b) and 9(c) are similar to those obtained in our measurements; other simulations also confirm the scale of these values.

In both simulation and experiment, the maximum power delivered to the load in the nonadiabatic regime can be obtained by using large driving powers P. As shown in Fig. 7(c), sometimes the maximum value is reached around the center of the rectification window. A combination of these findings suggests that a good value to start is a large value of P on the rectification step with some variations for optimization in the actual experiment. The estimated maximum $P_{out} = I_{stop}\overline{V} \approx 50\ \mu\text{A} \times 34\ \mu\text{V} = 1.7$ nW for $n = +1$ and $P_{out} \approx 3.3$ nW for $n = -1$ in Fig. 7 and $P_{out} \approx 5.7$ nW for $n = -1$ in Fig. 6. Note the difference from the adiabatic case where $\overline{V}$ tends to zero smoothly as a function of I_{ac}, so that $P_{out} \to 0$ too. In the nonadiabatic case the maximum P_{out} may be reached at the edge of the step as in Fig. 6.

VI. CONCLUSION

We implemented the Josephson vortex ratchet using an annular long Josephson junction equipped with current injectors used to create the ratchet potential and inject a fluxon into the junction. In comparison with our previous studies (and, actually, in comparison with most studies of ratchets in general) we have not only demonstrated rectification and some figures of merit in the idle regime, but also loaded the ratchet to study the maximum dc force that the ratchet can overcome

as well as its ac to dc power conversion efficiency in both quasistatic and nonadiabatic regimes.

In the quasistatic regime we derived the dependence of the stopping force $I_{stop}(I_{ac})$ analytically using a reasonable model for the IVC. This model predicts that, in order to increase the value of the stopping force (and other figures of merit), the amplitude of the ratchet potential should be rather large. The stopping force is directly related to the loading capability of a ratchet and to the maximum rectified power that it can deliver to the load. The maximum output power P_{out} is also reached at the upper end of the rectification window for intermediate values of I_{dc}. However, the ratchet works with maximum efficiency at the lower end of the rectification window. The ultimate efficiency that can be reached in principle is defined only by the asymmetry of the potential; see Eq. (20).

In the nonadiabatic regime, we have measured rectification curves and sometimes observed a transition between $n = +1$ and $n = -1$ dynamics with a small hysteresis. By applying an additional dc bias current I_{dc} in the rectification regime, we have measured the stopping force. Both I_{stop} and P_{out} have maxima near the upper edge of the rectification window. The support force, i.e., the current with the same sign compared to the rectification voltage, where the ratchet stops working does not change very drastically throughout the rectification window.

Therefore, if one wants to have a robust ratchet operation tolerant to additional bias currents, the ratchet should be operated at the upper end of the rectification window and the dc bias current (flowing to the load) should not exceed $I_{stop}(I_{ac})$.

ACKNOWLEDGMENTS

This work was supported by the Deutsche Forschungsgemeinschaft (Grant No. KO1303/7-1). M.K. acknowledges support by the Carl Zeiss Stiftung.

[1] R. P. Feynman, R. B. Leighton, and M. Sands, *The Feynman Lectures On Physics*, Vol. 1 (Addison-Wesley, Reading, MA, 1966).
[2] M. O. Magnasco, Phys. Rev. Lett. **71**, 1477 (1993).
[3] F. Jülicher, A. Ajdari, and J. Prost, Rev. Mod. Phys. **69**, 1269 (1997).
[4] P. Reimann, Phys. Rep. **361**, 57 (2002).
[5] P. Hänggi and F. Marchesoni, Rev. Mod. Phys. **81**, 387 (2009).
[6] S. Savel'ev, F. Marchesoni, P. Hänggi, and F. Nori, Phys. Rev. E **70**, 066109 (2004).
[7] L. Morales-Molina, F. G. Mertens, and A. Sánchez, Phys. Rev. E **73**, 046605 (2006).
[8] F. Falo, P. J. Martínez, J. J. Mazo, and S. Cilla, Europhys. Lett. **45**, 700 (1999).
[9] E. Trías, J. J. Mazo, F. Falo, and T. P. Orlando, Phys. Rev. E **61**, 2257 (2000).
[10] E. Goldobin, A. Sterck, and D. Koelle, Phys. Rev. E **63**, 031111 (2001).
[11] G. Carapella, Phys. Rev. B **63**, 054515 (2001).
[12] G. Carapella and G. Costabile, Phys. Rev. Lett. **87**, 077002 (2001).
[13] G. Carapella, G. Costabile, N. Martucciello, M. Cirillo, R. Latempa, A. Polcari, and G. Filatrella, Physica C **382**, 337 (2002).
[14] J. B. Majer, J. Peguiron, M. Grifoni, M. Tusveld, and J. E. Mooij, Phys. Rev. Lett. **90**, 056802 (2003).
[15] A. V. Ustinov, C. Coqui, A. Kemp, Y. Zolotaryuk, and M. Salerno, Phys. Rev. Lett. **93**, 087001 (2004).
[16] M. Beck, E. Goldobin, M. Neuhaus, M. Siegel, R. Kleiner, and D. Koelle, Phys. Rev. Lett. **95**, 090603 (2005).
[17] H. B. Wang *et al.*, Phys. Rev. B **80**, 224507 (2009).
[18] J. E. Villegas, S. Savel'ev, F. Nori, E. M. Gonzalez, J. V. Anguita, R. García, and J. L. Vicent, Science **302**, 1188 (2003).
[19] D. Cole, S. Bending, S. Savel'ev, A. Grigorenko, T. Tamegai, and F. Nori, Nat. Mater. **5**, 305 (2006).
[20] S. Ooi, S. Savel'ev, M. B. Gaifullin, T. Mochiku, K. Hirata, and F. Nori, Phys. Rev. Lett. **99**, 207003 (2007).
[21] P. Hänggi and R. Bartussek, in *Nonlinear Physics of Complex Systems—Current Status and Future Trends*, edited by J. Parisi, S. C. Müller, and W. Zimmermann, Lecture Notes in Physics Vol. 476 (Springer-Verlag, Berlin, 1996), p. 294.
[22] I. Zapata, R. Bartussek, F. Sols, and P. Hänggi, Phys. Rev. Lett. **77**, 2292 (1996).
[23] S. Weiss, D. Koelle, J. Müller, R. Gross, and K. Barthel, Europhys. Lett. **51**, 499 (2000).
[24] A. Sterck, S. Weiss, and D. Koelle, Appl. Phys. A **75**, 253 (2002).
[25] A. Sterck, R. Kleiner, and D. Koelle, Phys. Rev. Lett. **95**, 177006 (2005).
[26] A. Sterck, D. Koelle, and R. Kleiner, Phys. Rev. Lett. **103**, 047001 (2009).
[27] A. Davidson, B. Dueholm, B. Kryger, and N. F. Pedersen, Phys. Rev. Lett. **55**, 2059 (1985).
[28] A. Davidson, B. Dueholm, and N. F. Pedersen, J. Appl. Phys. **60**, 1447 (1986).
[29] A. V. Ustinov, T. Doderer, R. P. Huebener, N. F. Pedersen, B. Mayer, and V. A. Oboznov, Phys. Rev. Lett. **69**, 1815 (1992).
[30] N. Martucciello and R. Monaco, Phys. Rev. B **53**, 3471 (1996).
[31] A. V. Ustinov, Appl. Phys. Lett. **80**, 3153 (2002).
[32] B. A. Malomed and A. V. Ustinov, Phys. Rev. B **69**, 064502 (2004).
[33] A. V. Ustinov, Physica D **123**, 315 (1998).
[34] D. W. McLaughlin and A. C. Scott, Phys. Rev. A **18**, 1652 (1978).
[35] M. Borromeo, G. Costantini, and F. Marchesoni, Phys. Rev. E **65**, 041110 (2002).
[36] J.-F. Chauwin, A. Ajdari, and J. Prost, Europhys. Lett. **32**, 373 (1995).
[37] P. Jung, J. G. Kissner, and P. Hänggi, Phys. Rev. Lett. **76**, 3436 (1996).
[38] J. L. Mateos, Phys. Rev. Lett. **84**, 258 (2000).
[39] J. Mateos, Physica A **325**, 92 (2003).
[40] W.-S. Son, I. Kim, Y.-J. Park, and C.-M. Kim, Phys. Rev. E **68**, 067201 (2003).
[41] E. Goldobin, http://www.geocities.com/SiliconValley/Heights/7318/StkJJ.htm.